Enhancing strong-field-induced molecular vibration with femtosecond pulse shaping

M. Bitter,[1] E. A. Shapiro,[2] and V. Milner[1]
[1]*Department of Physics & Astronomy and The Laboratory for Advanced Spectroscopy and Imaging Research (LASIR)*
[2]*Department of Chemistry, The University of British Columbia, Vancouver, Canada*
(Received 15 August 2012; published 17 October 2012)

This work investigates the utility of femtosecond pulse shaping in increasing the efficiency of Raman excitation of molecules in the strong-field interaction regime. We study experimentally and theoretically the effect of pulse shaping on the strength of nonresonant coherent anti-Stokes Raman scattering in iodine vapor at laser intensities exceeding 10^{13} W/cm^2. We show that unlike the perturbative case, shaping strong nonresonant laser pulses can increase the signal strength beyond that observed with the transform-limited excitation. Both adiabatic and nonadiabatic schemes of excitation are explored, and the differences of their potential in increasing the excitation efficiency are discussed.

DOI: 10.1103/PhysRevA.86.043421 PACS number(s): 33.80.Wz, 42.50.Hz

I. INTRODUCTION

The broad spectral bandwidth of ultrashort laser pulses is often used to excite coherent molecular wave packets consisting of a number of rotational and vibrational eigenstates. Studying the dynamics of an excited wave packet on the femtosecond time scale represents a powerful approach to molecular spectroscopy [1]. Femtosecond spectroscopy benefits from the technology of pulse shaping [2], which offers selectivity and control of molecular excitation and has been successfully implemented in various spectroscopic applications of nonlinear optics such as multiphoton absorption and ionization, stimulated and coherent anti-Stokes Raman scattering, sum-frequency generation, and four-wave mixing (for a recent review of the topic, see, e.g., [3]).

In the weak-field regime of multiphoton, for example, Raman, excitation of molecules, that is, when molecular states are not changed significantly by the applied laser fields and the perturbation theory holds, the complex amplitudes of the excited molecular states are proportional to the corresponding resonant spectral components of the two-photon excitation field [4,5]. In the absence of intermediate resonances, an upper bound on the *absolute efficiency* of exciting a particular mode is set by the available laser intensity and is reached with unshaped transform-limited (TL) laser pulses. Hence, improving the efficiency of an off-resonance Raman process in the perturbative regime can be achieved by increasing the laser intensity, whereas shaping the spectrum of the driving field can only suppress rather than enhance the excitation at any given frequency. Stronger laser fields modify the molecular field-free states, most importantly via ac Stark shifts, often suppressing the rate of the target transition [6–9]. As a result, unshaped pulses no longer provide maximum efficiency of transferring molecules to the target vibrational state in the strong-field limit.

In this work, we investigate the utility of femtosecond pulse shaping to increase the magnitude of nonresonant vibrational excitation. We explore, both experimentally and theoretically, the efficiency of exciting vibrational wave packets in the ground electronic state of molecular iodine subject to strong laser pulses ($>10^{13}$ W/cm^2). Evaluating the efficiency of strong-field induced vibrational excitation by means of coherent anti-Stokes Raman scattering (CARS), we demonstrate that pulse shaping can lead to the enhancement of the nonlinear spectroscopic signal by at least 50%.

Two qualitatively different approaches are analyzed. First, we suppress strong-field effects (such as ac Stark shifts) that may reduce the efficiency of the CARS process. In contrast to the feedback-loop-based adaptive control [6,10,11], we achieve this by applying pre-determined pulse shapes to the excitation pulses in such a way as to lower the instantaneous field strength while preserving the amplitude of the two-photon field at the frequency of Raman resonances.

In the second approach we try to employ the technique of adiabatic passage (AP) to enhance off-resonance vibrational excitation by making use of, rather than avoiding, strong-field effects. Nonadiabatic population transfer is very sensitive to the fluctuations of the laser parameters like intensity or pulse duration [12]. In AP, one exploits an adiabatic time evolution to improve the robustness of the process and enhance the efficiency of population transfer. Earlier works have demonstrated a number of successful implementations of adiabatic transfer in two- and three-level systems driven by resonant laser radiation [13–18]. Previous studies questioned the utility of AP in multilevel molecular systems interacting with strong femtosecond pulses [19,20]. In this work we put to test the techniques of two-photon rapid adiabatic passage (RAP [21,22]), stimulated Raman adiabatic passage (STIRAP [13]), and "piecewise AP" [23,24]. The latter approach has been proven successful in atomic systems [17,25] but has not been implemented with molecules.

We use femtosecond CARS to determine the efficiency of vibrational excitation in the ground electronic state of molecular iodine. Two strong laser pulses, pump and Stokes, with frequencies ω_{p} and ω_{S} and intensities exceeding 10^{13} W/cm^2, prepare the vibrational coherence via an off-resonance two-photon Raman transition. A weak probe pulse with frequency ω_{pr}, separated in time from pump and Stokes, scatters off this coherence generating the anti-Stokes field at $\omega_{aS} = \omega_p - \omega_S + \omega_{pr}$. The detected CARS signal at ω_{aS} serves as a quantitative measure of the degree of vibrational excitations, and its dependence on the spectral shapes of both pump and Stokes pulses is explored.

II. CHOICE OF PULSE SHAPING

The spectral phase of both pump and Stokes excitation fields is shaped simultaneously in such a way as to (1) suppress the strong-field-induced level shifts or (2) initiate an AP process. In both cases, we aim at increasing the strength of the CARS signal. The important difference between the two approaches lies in the two-photon pump-Stokes field. In scenario one, the spectral power densities at the desired Raman transition frequencies are maintained while the peak intensities of the pulses are reduced. Thus, the detrimental strong-field Stark shifts are minimized. In the second scenario, not only the field amplitudes of undesired frequencies but also those of the target Raman transitions are lower than in the TL case.

A. Linear frequency chirping

Equal-frequency chirps applied to both pump and Stokes pulses result in the narrowing of the two-photon excitation spectrum around a constant frequency which is tuned to the frequency of the target vibrational transition Ω_0. The spectral power density at that Raman transition is kept constant, whereas the peak power of the individual pulses can be substantially lowered.

Linear chirping of the instantaneous frequency of pump and Stokes fields $\omega_{p,S}(t) = \omega_{0(p,S)} + \alpha t$ is achieved by applying the parabolic spectral phase masks by means of two pulse shapers:

$$\varphi_{p,S}(\omega) = -\tfrac{1}{2}\alpha'(\omega - \omega_{0(p,S)})^2. \quad (1)$$

ω_{0p} and ω_{0S} are the central frequencies of pump and Stokes pulses, respectively. In the case of a large chirp, that is, when the chirped pulse is much longer than its Fourier-transform limit, the spectral and temporal chirps are related as $\alpha \approx 1/\alpha'$ [22]. An example of the temporal amplitude and phase before and after linear chirping is shown in Fig. 1(a). In comparison to a TL pulse, the peak amplitude of the shaped pulse drops as the pulse is stretched in time in linear proportion with α'. The instantaneous frequency of the two-photon excitation spectrum of two linearly chirped pump and Stokes pulses with an equal chirp rate α remains constant, $\Omega(t) := \omega_p(t) - \omega_S(t) = \omega_{0p} - \omega_{0S}$, as shown in Fig. 2(a). Together with the two-photon field spectrum, we plot all possible Raman transitions in room-temperature iodine vapor within the accessible spectral bandwidth. Initial thermal population distribution among the vibrational levels $v = 0,1,2,\ldots$ is taken into account. Vibrational resonances are broadened due to the thermal molecular rotation. We do not resolve the rotational spectrum in our experiments. The excitation line width is inversely proportional to the applied chirp α', whereas its frequency can be tuned by a variable time delay between pump and Stokes pulses. In CARS microscopy this method is known as spectral focusing [26]. In our experiments, $\alpha' = 50\,000$ fs^2 is chosen to match the excitation line width with the rotational broadening of the vibrational transitions.

B. Sinusoidal phase modulation

Narrowing of the two-photon spectrum around the target Raman frequency Ω_0 requires the spectral phase of pump and Stokes pulses to be identical around ω_{0p} and $\omega_{0S} = \omega_{0p} - \Omega_0$, respectively, as in the case of equal-frequency chirps described above. If the goal is to excite a vibrational wave packet consisting of several eigenstates, the applied phase mask must be periodic in frequency, with a period matching the vibrational period of a molecule [27–29].

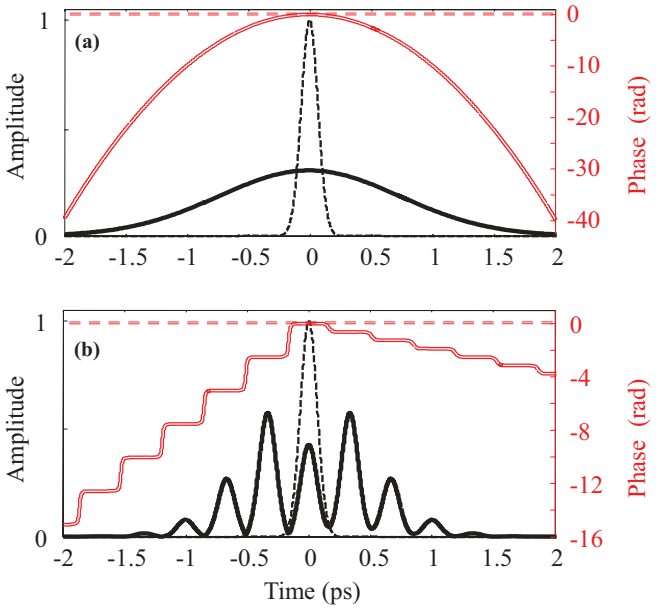

FIG. 1. (Color online) Temporal profile of TL (dashed lines) and shaped (solid lines) femtosecond pulses with the electric field amplitude (black single lines) and phase (red double lines). (a) Linearly chirped pulse with $\alpha' = 50\,000$ fs^2; (b) sinusoidal phase modulation with $A = 1.65$, $T = 334$ fs.

Sinusoidal phase modulation represents one of the most popular methods of periodic shaping [18,23,24,30,31]. In this case,

$$\varphi_{p,S}(\omega) = A\sin[(\omega - \tilde{\omega}_{p,S})T], \quad (2)$$

where T describes the modulation period and A its amplitude. $\tilde{\omega}_p$ and $\tilde{\omega}_S$ are the central modulation frequencies of pump and Stokes pulses, respectively. In the time domain, this spectral shaping results in a train of pulses, with each pulse being an exact replica of the initial TL pulse, and the time delay between the pulses defined by T [Fig. 1(b)]. By matching or mismatching the train period with the period of molecular vibration, the latter can be either enhanced or suppressed. Weak-field vibrational control by means of periodic pulse trains has been successfully demonstrated [28,29,32,33]. In the strong-field regime considered in this work, breaking the initial pulse into a train of weaker pulses serves the purpose of suppressing the detrimental multiphoton processes prohibiting the transfer of molecules to the target state.

If an identical sinusoidal phase modulation is applied to both pump and Stokes excitation pulses, the two-photon spectrum shows periodic peaks with flat phase across them, see Fig. 2(b). Unlike the case of a frequency chirp, all three vibrational bands are now excited with the maximum possible amplitude (set by the available bandwidth) if the period T is a multiple integer of the vibrational period. The modulation amplitude A determines the number of pulses in the pulse

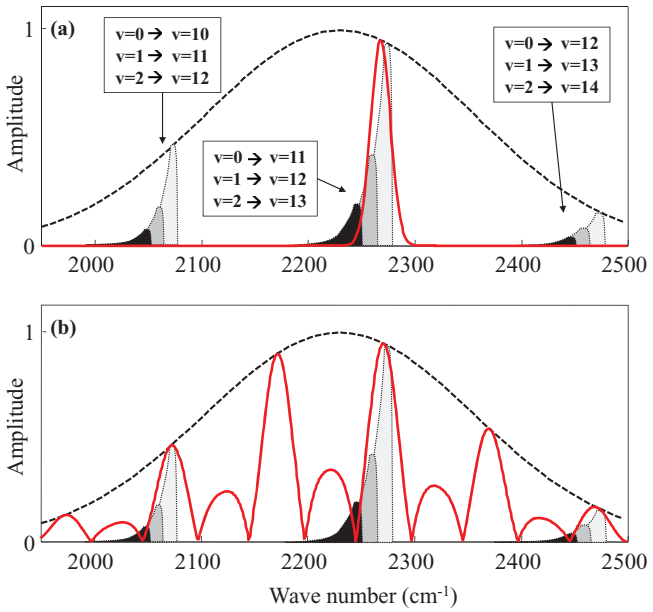

FIG. 2. (Color online) Raman spectrum at $\omega_p - \omega_S$ for TL pulses (black dashed line) and shaped pulses (red solid line). All Raman transitions (rotationally broadened into bands) and their strengths are indicated according to thermal Boltzmann distribution at 100 °C: initial states $v = 0$ (white area), $v = 1$ (gray area), and $v = 2$ (black area). (a) Linearly chirped pulses with $\alpha' = 50\,000$ fs^2; (b) sinusoidal phase modulation with $A = 1.65$, $T = 334$ fs.

train, as well as the line width of the spectral peaks in the two-photon spectrum [30]. Similarly to the parabolic phase shaping described above, we tune the value of A for the best coverage of the rotationally broadened Raman transitions in iodine. The central modulation frequencies $\tilde{w}_{p,S}$ in Eq. (2) control the absolute position of the peaks in the two-photon spectrum.

C. Pulse shaping for adiabatic passage

In RAP, the instantaneous frequency of the excitation field is swept across the target transition frequency [22,34]. In the case of a Raman process, this corresponds to chirping the two-photon frequency. Applying linear frequency chirps with opposite signs to pump and Stokes fields $\alpha_p = -\alpha_S = \alpha$, results in a linearly chirped two-photon field with an instantaneous frequency of $\Omega(t) = \omega_p(t) - \omega_S(t) = \omega_{0p} - \omega_{0S} + 2\alpha t$.

The technique of STIRAP relies solely on a relative time delay between pump and Stokes pulses. Hence, no pulse shaping is necessary. The pulse trains needed for piecewise STIRAP can be implemented via amplitude and phase shaping according to the method described in Ref. [17] (see also Fig. 6).

III. NUMERICAL ANALYSIS

In our experimental detection scheme based on CARS [Fig. 3(a)], the signal from a *single* final state $|v_f\rangle$ is proportional to the square of the coherence between that state and the initial vibrational state $|v_0\rangle$, that is, the square amplitude of $|v_0\rangle\langle v_f|$ in the density matrix. Since the rate of both collisional and rotational decoherence is negligible on the experimentally realized time scale of a few picoseconds,

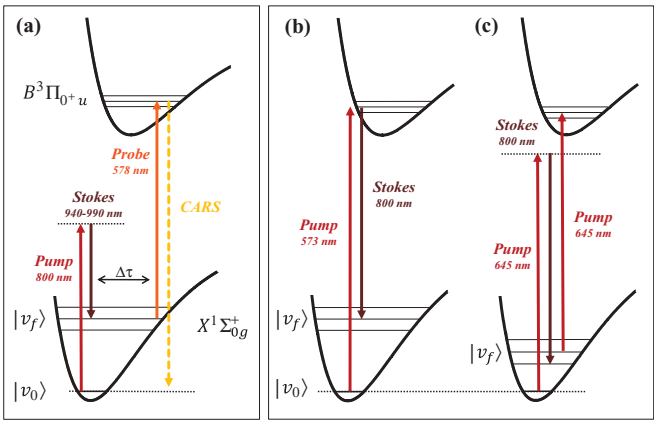

FIG. 3. (Color online) Vibrational excitation schemes of iodine molecules, discussed in this work. (a) Pump and Stokes pulses are off-resonance with the excited electronic B state and generate vibrational coherence between $|v_0\rangle$ and $|v_f\rangle$ in the ground X manifold, which is probed after a variable time delay $\Delta\tau$. (b), (c) Pump and Stokes pulses are resonant with a single-photon electronic transition $X \leftarrow B$.

and the target population is small, the signal magnitude is proportional to the population of the final state. We therefore base our numerical analysis on calculating the transfer of population from the ground vibrational state, predominantly populated at our experimental conditions, to higher vibrational states, driven by strong pump and Stokes excitation fields. For a *coherent wave packet* consisting of several vibrational final states, the observed CARS signal oscillates as a function of the arrival time of probe pulses (see Results section below). Rather than model this time behavior, we assume that the time-averaged signal is proportional to the sum of the calculated populations.

To calculate the redistribution of the vibrational population as a result of the strong-field interaction, we solve the time-dependent Schrödinger equation in the eigenstate basis. The propagation routine does not employ the rotating wave approximmation and thus automatically accounts for ac Stark shifts. We take into account transitions between two electronic manifolds of I_2, $X^1\Sigma^+_{0g}$ and $B^3\Pi_{0+u}$. Both potentials are modeled as Morse oscillators [35]. The electronic transition dipole moment is set to an approximate value of 1 D, while the Franck-Condon factors for the $B \leftarrow X$ transitions are calculated numerically. While such modeling is not fully accurate for high vibrational states of iodine [36], it can provide a good qualitative description of the quantum dynamics. Quantitatively, in our simulations the strong-field effects arise at intensities somewhat lower than those observed experimentally.

In the main set of calculations, we explore the simplest case of a strongly driven off-resonance Raman excitation. We avoid one-photon resonances and set the central wavelength of the pump pulse to $\lambda_p = 800$ nm, whereas the Stokes pulse is varied between $\lambda_S = 940$ and 990 nm. Importantly, neither pump nor Stokes photons have enough energy to drive a resonant transition between either $|v_0\rangle$ or $|v_f\rangle$ and the vibrational states of the B manifold. Various multiphoton interaction pathways that couple $|v_0\rangle$ to other electronic and vibrational states become intertwined in the strong-field limit. The population

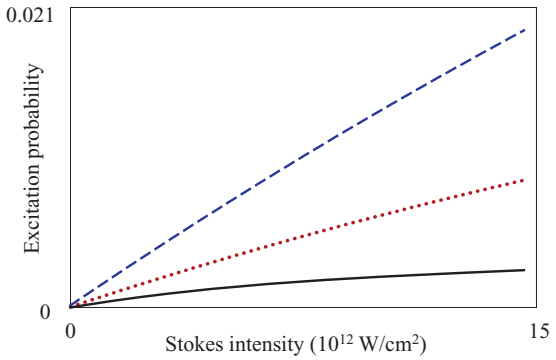

FIG. 4. (Color online) Raman excitation probability as a function of Stokes intensity. The excitation schemes are as follows: TL pulses (black solid line), pump and Stokes pulses linearly chirped (blue dashed line), pump and Stokes pulses shaped with a sinusoidal phase mask (red dotted line).

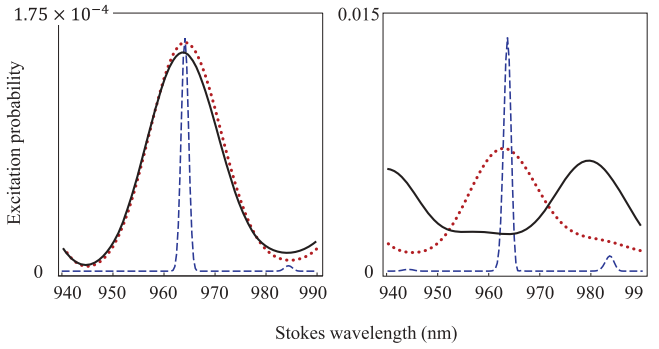

FIG. 5. (Color online) Raman excitation probability as a function of Stokes wavelength. (Left) Both pump and Stokes intensities are set to 10^{12} W/cm^2. (Right) Both intensities are set to 10^{13} W/cm^2. Line assignment is the same as in Fig. 4.

transfer is influenced by the time-dependent Stark shifts which move various vibrational levels in and out of resonance with different components of the Raman excitation spectrum.

The interplay of various nonlinear strong-field processes, most notably dynamic Stark shifts, makes the perturbative approach inapplicable. The transition amplitudes cannot be correctly calculated by expanding the transition matrix elements to any order of the perturbation theory. Note that the strong-field regime does not necessarily imply large transition amplitudes. Rather, it leads to the suppression of Raman transitions into target states, and thus to the observed suppression of CARS signal.

We first focus on the pulse shapes designed to reduce the peak intensity of the excitation pulses, while enabling the excitation of either a single vibrational level (quadratic spectral phase mask) or a superposition of levels (sinusoidal spectral phase mask). In the former case, a linear chirp with $\alpha' = 46\,000$ fs^2 stretches pump and Stokes pulses to $\sim$1 ps duration. In the second case, the sinusoidal mask of Eq. (2) with $A = 1.23$ and $T = 312$ fs leads to a pulse train consisting of five pulses separated in time by twice the oscillation period of a wave packet composed of the vibrational states adjacent to $v_f = 10$. The factor of 2 is introduced for an easier distinction of individual pulses in the resulting pulse train.

Figure 4 demonstrates the dependence of the Raman transfer efficiency on laser intensity. Here, pump intensity (I_p) is fixed at 1.5×10^{13} W/cm^2 while Stokes intensity (I_S) is scanned. The Stokes wavelength is set to 964 nm, corresponding to a strong two-photon resonance with $v_f = 10$. We compare the effect of 130-fs $\sin^2 t/t_0$-shaped TL pump and Stokes pulses [full width at half maximum (FWHM) of the intensity profile] and that of the shaped pulses simulated with a numerical pulse shaper. As the experimental detection is carried out with a broadband probe and therefore does not offer frequency resolution, we plot the sum of populations in the target manifold, $v = 6, \ldots, 13$, rather than the populations of the individual levels. This range is wide enough to include all the states covered by the excitation bandwidth in the presence of strong-field Stark shifts. On the other hand, it does not include those states which can be populated in pump-pump and Stokes-Stokes Raman transitions in the presence of Stark shifts.

The lower curve in Fig. 4 illustrates the main motivation of this work: The efficiency of the Raman excitation driven by high-intensity TL pulses saturates, setting an upper bound on the magnitude of the CARS signal. The saturation stems from an oscillatory behavior of the individual target populations, which takes over the linear (with I_S) growth of population anticipated in the weak-field limit. We associate these population oscillations with an interplay of population transfer with multiple ac Stark shifts which dynamically change the instantaneous spectrum of the molecular states dressed by the strong laser field. We note that on the scale of laser intensities considered in this work, the oscillation amplitudes are typically of the order of 1%–2% of the total population, which explains the low total efficiency of the Raman excitation plotted in Fig. 4. If the two-photon field is resonant with a Raman transition to a certain vibrational state $|v_f\rangle$, then the linear frequency chirping of pump and Stokes pulses provides the largest suppression of the strong-field saturation (dashed curve in Fig. 4). Raman excitation by a train of pump/Stokes pulse pairs (sinusoidal spectral mask) showed an intermediate level of saturation (dotted curve in Fig. 4). We attribute this difference in performance to the fact that for a given pulse energy, frequency chirping results in the lowest peak intensity and therefore better suppression of the detrimental strong-field effects discussed above.

Further insight can be gained by calculating the transfer efficiency as a function of the central Stokes frequency, ω_{0S}. The results are shown in Fig. 5. In the weak-field regime (left panel), the transition strength is defined by the corresponding resonant component of the two-photon pump-Stokes spectrum. Since the peak spectral amplitudes are equal for all three pulse shapes, the population transfer to a single state $|v_f\rangle$ is equally efficient when $\omega_{0p} - \omega_{0S} = (E_f - E_0)/\hbar$, where E_f and E_0 are the energies of the excited and ground vibrational states, respectively. In this figure, the Raman resonance with $v_f = 10$ lies at $\lambda_S = 964$ nm. Raman transitions to the neighboring $v_f = 9$ and $v_f = 11$ are much weaker due to oscillations in the two-photon coupling strength. For the frequency-chirped pulses, the two-photon spectrum is narrower than in the case of TL pulses [see Fig. 2(a)], resulting in a faster drop of the transfer efficiency away from the resonance. The two-photon

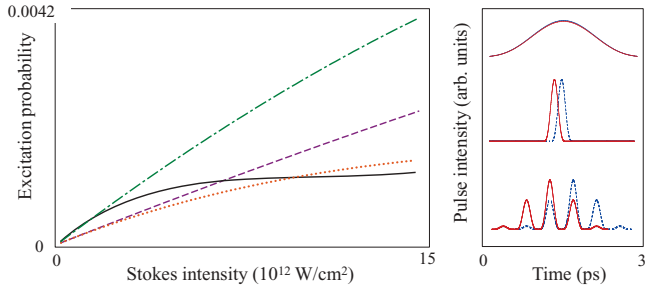

FIG. 6. (Color online) (Left) Raman excitation probability as a function of Stokes intensity. The excitation schemes are as follows RAP (purple dashed line), STIRAP (orange dotted line), piecewise STIRAP (green dash-dotted line), and TL pulses (black solid line). (Right) Schematic view of the intensity profiles of pump (blue dashed line) and Stokes (red solid line) pulses used in the calculations of RAP (top), STIRAP (middle), and piecewise STIRAP (bottom).

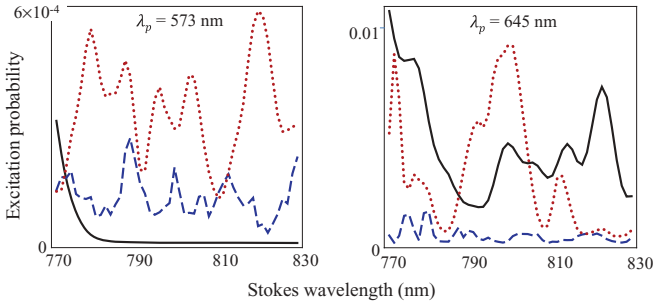

FIG. 7. (Color online) Raman excitation probability as a function of Stokes wavelength in two cases of resonant excitation schemes shown in Fig. 3 [left, Fig. 3(b); right, Fig. 3(c)]. Line assignments are as in Figs. 4 and 5. The target manifold is extended to $v = 6, \ldots, 17$ in order to account for all Raman transitions at the given pump and Stokes wavelengths. Both intensities are set to 10^{13} W/cm^2.

spectrum of the pump-Stokes pulse train has a much wider maximum [37].

The right panel of Fig. 5 shows the calculated transfer efficiency in the strong-field limit. Dynamic Stark shifts modify the line shape and lead to a significantly lower population of the target vibrational manifold. The vibrational excitation by a train of pulses is suppressed to a much lower degree. Indeed, the intensity of pulses in the train is lower than that of the original femtosecond pulse and the strong-field effects are correspondingly weaker. Finally, chirped pulses correspond to the highest population transfer. The absence of a visible line broadening in this case points to the complete elimination of the detrimental strong-field effects.

Our calculations do not indicate that the adiabatic techniques of two-photon RAP [22,34], STIRAP [11] or piecewise STIRAP [23,24] are feasible. Indeed, AP is usually used to improve the robustness of an already high transfer rate. The left panel of Fig. 6 investigates the strong-field transfer for the three adiabatic schemes. The intensity profiles are shown in the right panel with wavelengths and intensities similar to those in Fig. 4. For RAP, we show the transfer efficiency with pump and Stokes fields chirped in the opposite directions with $|\alpha'| = 46\,000$ fs^2. This shaping results in a frequency chirp of the two-photon pump-Stokes field. For STIRAP, TL Stokes pulses precede TL pump pulses by 130 fs. For piecewise STIRAP, we consider two pulse trains obtained via sinusoidal spectral phase modulation, as described above, and shifted relative to each other in the counterintuitive order by the pulse train period [23,24]. In all three cases, the two-photon spectrum is lower than that of a TL pulse. Hence, the transfer efficiency at small intensities is lowered by the applied pulse shaping. At high intensities, the transfer efficiency is only slightly higher than that of TL pulses, but still is significantly lower than that achieved by the nonadiabatic techniques in Fig. 4.

Finally, we compare the results of the off-resonance excitation regime, with the two resonant cases, where a single-photon electronic excitation from either v_0 (case 1, $\lambda_p = 573$ nm, $\lambda_S \sim 800$ nm) or v_f (case 2, $\lambda_p = 645$ nm, $\lambda_S \sim 800$ nm) is energetically allowed, as illustrated in Figs. 3(b) and 3(c), respectively. The choice of these wavelengths is based on our experimental settings and on the previous studies [19,20]. In both cases, one-photon coupling to the excited electronic state at the pump frequency significantly complicates the population dynamics. The dependance of the transfer efficiency on the wavelength, is irregular due to the interplay of time-dependent ac Stark shifts and a single-photon escape of population into the B manifold. In the first case, the overall transfer efficiency at high intensities can be several orders of magnitude lower than that in the far off-resonance arrangement considered in the main set of calculations. In the second case (previously studied in Refs. [19,20]), the efficiency can be either below or slightly above that of the far off-resonance arrangement, depending on the exact pump and Stokes wavelengths. However, the dependence on the laser parameters remains erratic (see Fig. 7). The efficiencies observed in our calculations are lower than those reported in Refs. [19,20]. In our calculation, the target population transfer into v_f is hindered by one-photon coupling to the excited electronic state at the pump frequency.

IV. EXPERIMENTAL STUDY

A. Experimental setup

A Ti:sapphire-based laser system (SpitFire Pro, Spectra-Physics) produces 2 mJ 130 fs pulses at 800 nm and 1 kHz repetition rate. These pulses serve as pump, whereas one optical parametric amplifier (TOPAS, Light Conversion) generates Stokes pulses at a wavelength of 973 nm and another OPA (OPA-800C, Spectra Physics) generates probe pulses at 578 nm.

All three pulses are aligned collinearly and are spatially overlapped inside a vapor cell filled with I_2 at variable temperature [see Fig. 8(a)]. At 100 °C, used in this work, the vapor pressure is 43 Torr [38]. Collinear geometry is implemented to increase the interaction length and reduce the effect of spatial averaging over the Gaussian beam profiles. The latter is also achieved by making the focal size of the probe beam smaller than the size of the other beams. With a 30-cm focusing lens, peak intensities of up to 5×10^{13} W/cm^2 for pump and Stokes pulses and 2×10^{12} W/cm^2 for probe pulses are obtained. Spatial filtering in the detection channel is used to eliminate a majority of the fluorescence background. In order to filter the output anti-Stokes beam from the incident beams, we use polarization and spectral filtering, as shown in

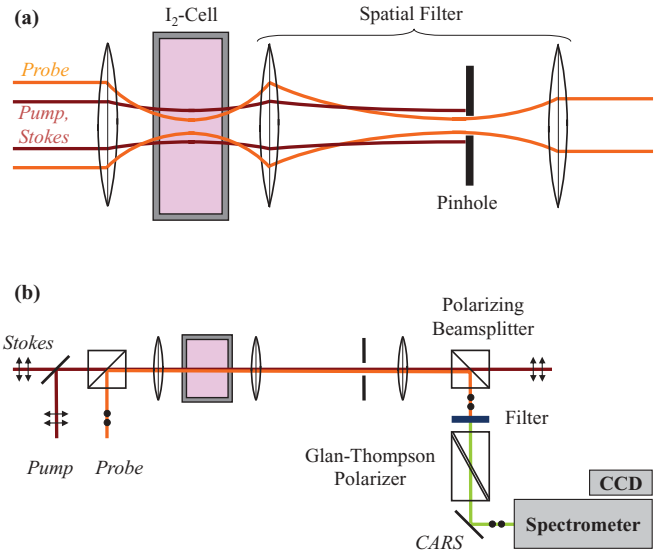

FIG. 8. (Color online) Experimental setup. (a) Collinear CARS geometry with spatial filtering. (b) Use of polarizing optics and spectral filtering to separate CARS signal from the excitation pulses.

Fig. 8(b). Probe pulses are linearly polarized in the orthogonal direction to pump and Stokes pulses. Hence, the anti-Stokes polarization does not coincide with that of the strong excitation fields, enabling one to block the latter while passing through part of the CARS signal [39]. The filtered signal is sent to a spectrometer equipped with a cooled (−40 °C) charge-coupled device (CCD) camera. Two delay lines are used to vary the relative arrival time of pump, Stokes and probe pulses. Pump and Stokes pulses are shaped by two separate pulse shapers implemented in a standard $4f$ geometry [2].

B. Results

To evaluate the effect of strong excitation fields, we start by detecting the output spectrum in the absence of probe pulses. The observed spectrum, shown in Fig. 9(b), is very broad and covers wavelengths above 400 nm. It corresponds to spontaneous emission following the process of two-photon absorption (TPA) in which any combination of two photons from the high-intensity pump and Stokes fields are absorbed. The 400-nm cutoff is determined by the maximum energy from the absorption of two 800-nm pump photons. If only pump or Stokes photons are present, the fluorescence signal shows a quadratic dependency on the intensity of the corresponding laser beam. The fluorescence signal stemming from TPA of one pump and one Stokes photon shows a linear dependence on the intensity of both laser beams. It provides the main contribution to TPA [Fig. 9(a)]. This is expected since the two-photon excitation amplitude scales as $(E_p + E_S)^2 = E_p^2 + E_S^2 + 2E_pE_S$, resulting in a fourfold enhancement of the intensity dependence on I_pI_S [here $E_p(I_p)$ and E_S (I_S) are the electric field amplitude (intensity) of pump and Stokes pulses, respectively]. The exact proportionality factor is a function of the frequency-dependent Frank-Condon factors. The strong peak at 678 nm is due to the nonresonant four-wave mixing process with two pump photons and one Stokes photon at frequency $2\omega_p - \omega_S$.

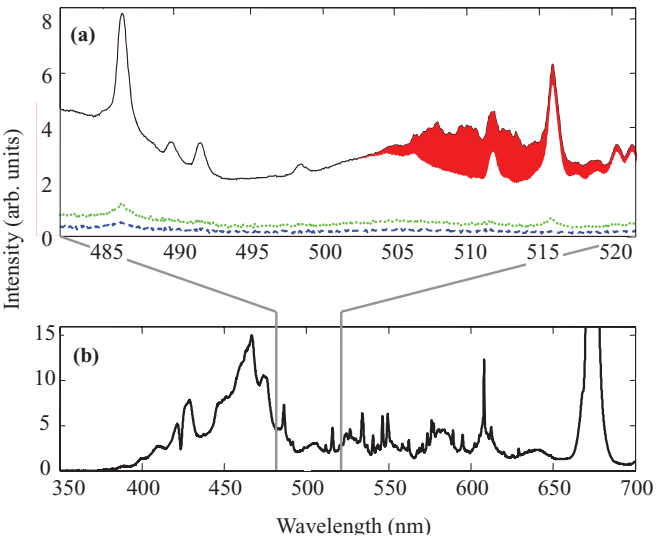

FIG. 9. (Color online) Fluorescence spectrum of iodine due to strong pump and Stokes excitation. (a) Detected signal in the wavelength range from 482 to 522 nm stemming from TPA of Stokes (blue dashed), TPA of pump (green dotted), and TPA of mixed pump and Stokes (black solid). CARS signal is shown on top of the fluorescence curve (red shaded area). (b) Fluorescence spectrum in the range from 350 to 700 nm.

Strong two-photon fluorescence, comparable in magnitude to the detected CARS signal even after both spatial and polarization filters have been applied [Fig. 9(a)], reflects a high degree of two-photon coupling responsible for the detrimental Stark shifts. Suppressing the TPA-induced fluorescence with pulse shaping can be considered as an indirect evidence of lowering the influence of strong-field effects on the target Raman excitation. Both the linear frequency chirp and the sinusoidal phase modulation drastically reduce the fluorescence background due to the narrowing of the two-photon spectrum discussed earlier in the text. The effect is shown in Fig. 10.

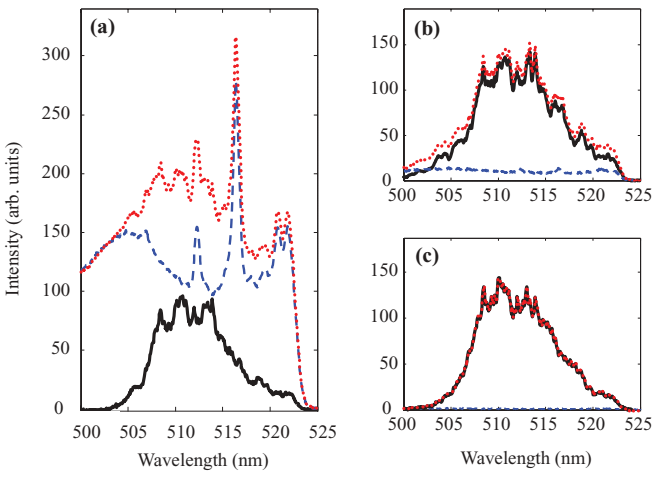

FIG. 10. (Color online) Detected spectrum with strong pump and Stokes fields and a weak probe field (red dotted line), output spectrum in the absence of probe pulses (blue dashed line), CARS signal derived as the difference of the two spectra (black solid line). Pump and Stokes pulses are (a) TL, (b) modulated with a sinusoidal phase, (c) linearly chirped.

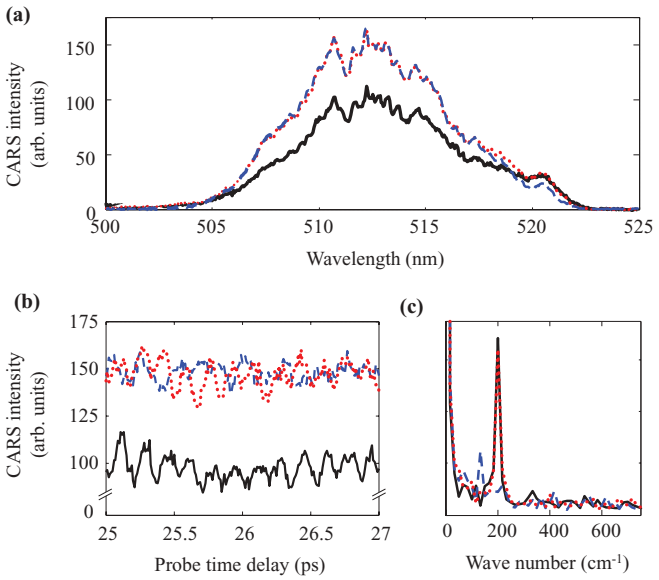

FIG. 11. (Color online) Comparison of CARS intensity with different excitation schemes Pump and Stokes pulses are TL (black solid line), linearly chirped (blue dashed line), or shaped with a sinusoidal phase mask (red dotted line). (a) CARS spectrum, (b) CARS signal as a function of the probe time delay, and (c) the corresponding Fourier spectra.

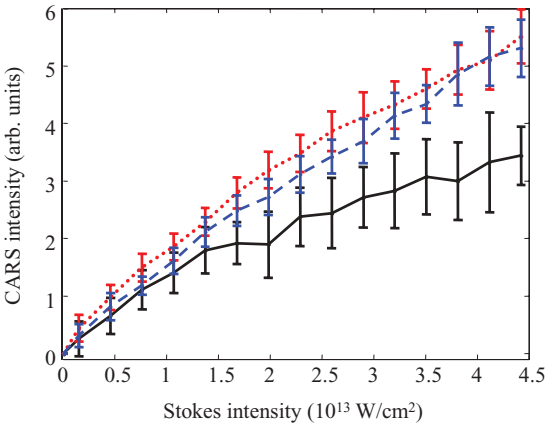

FIG. 12. (Color online) CARS intensity as a function of Stokes intensity with $I_p = 5 \times 10^{13}$ W/cm^2. Line assignments are the same as in Fig. 11.

As expected, linear chirping achieves better suppression of fluorescence, since the two-photon spectrum has fewer spectral components. In contrast to the suppressed TPA, the intensity of the CARS signal is rising, confirming the above argument about the mechanism of the strong-field induced saturation.

In Fig. 11, we plot the detected CARS signal obtained by subtracting the fluorescence background from the measured spectrum. We note that in this spectral region (i.e., around $\omega_p - \omega_S + \omega_{pr}$), the signal is free of nonresonant background since probe pulses are delayed by about 25 ps with respect to the temporal overlapping pump and Stokes pulses. The maximum available energy of the excitation pulses corresponds to peak intensities of $I_{p,S} = 5 \times 10^{13}$ W/cm^2 of the unshaped TL pulses. As can be seen in plots (a) and (b) of Fig. 11, both phase masks (quadratic and sinusoidal) result in an almost identical signal enhancement by about 50% in comparison to the case of the unshaped excitation.

The dependence of the CARS signal on the probe arrival time is plotted in Fig. 11(b). Aside form the similar difference in the absolute signal strength, we note that the oscillations of the excited vibrational wave packet, clearly seen in the case of the TL excitation, are preserved in the case of the sinusoidal phase modulation and suppressed in the case of the linear frequency chirping. The Fourier spectra in Fig. 11(c) reveal a peak at 200 cm^{-1}. This corresponds to a vibrational wave packet consisting of $v_f = 10, 11$, and 12 with an oscillation period of 167 fs. The peak is suppressed when frequency-chirped pulses are used. The small peak at ~135 cm^{-1} is an artifact due to the spectral phase wrapping in the pulse shaper. The observed effects are different from a well-known feature of the weak-field regime, where the excitation amplitude is linearly proportional to the amplitude of the two-photon field at resonant frequencies. Although the sinusoidal phase modulation does not change the spectral amplitude at the frequencies of the available Raman transitions [see Fig. 2(b)], it results in a substantial signal gain while allowing us to excite a coherent wave packet. On the other hand, the observed signal enhancement with the frequency-chirped pump and Stokes pulses is accompanied by the two-photon spectrum narrowing [Fig. 2(a)] and a consequent loss of the wave packet oscillations.

By scanning the intensity of the Stokes beam in Fig. 12, we observe the effect of pulse shaping above approximately 1.5×10^{13} W/cm^2 when the signal from the unshaped TL excitation starts to slow down. We attribute this onset of saturation to the deleterious strong-field effects, which are suppressed when the pulses are shaped. In the latter case, the signal keeps growing almost linearly exceeding the unshaped limit by about 50%. In agreement with recent work [40], strong-field effects and therefore the possibility of coherent control are found even if the response of the system (all three curves in Fig. 12) appears almost linear. Our numerical analysis suggests that frequency chirping should provide the highest CARS signal (see Fig. 4), whereas in the experiment, the two spectral masks result in a similar performance. In the simulations, we set the Stokes wavelength to match the peak of the two-photon spectrum with a Raman resonance. In the experiment, however, the wavelengths cannot be changed easily and the frequencies are matched by introducing a delay between pump and Stokes pulses (see also next paragraph). This delay reduces the two-photon spectral amplitude, since it is shifted from the maximum of the two-photon spectrum, thus lowering the signal. In the case of the sinusoidal phase modulation, the exact overlap of the two-photon spectrum with the Raman transition frequencies is easily maintained by adjusting the central modulation frequencies $\tilde{\omega}_{p,S}$ of Eq. (2) with pump and Stokes pulse shapers.

Following our numerical analysis, we examine the techniques of RAP and STIRAP in both the off-resonance and near-resonance cases. In the off-resonance case, that is, with the same choice of pump and Stokes wavelengths as before [$\lambda_p = 800$ nm, $\lambda_S = 973$ nm, Fig. 3(a)], we find no evidence of the AP enhancement of CARS signal. The search for STIRAP is carried out by scanning the relative timing between TL pump and Stokes pulses. Figure 13 shows the experimentally

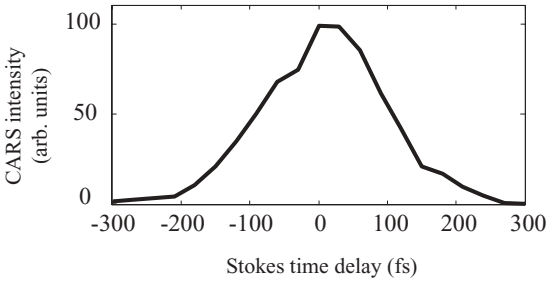

FIG. 13. CARS intensity as a function of the pump-Stokes time delay, implemented with TL pulses in the far off-resonance excitation scheme of Fig. 3(a).

detected CARS signal as a function of the time delay between the two pulses. To within our time resolution, the strongest CARS signal is observed with a perfect overlap of pulses, rather than at a nonzero time delay required by STIRAP. As required for RAP, we chirp pump and Stokes fields in opposite directions and observe CARS intensity always decreasing below the TL limit (not shown here). This agrees with the perturbative, rather than adiabatic, description of the Raman process. As discussed earlier in the text, opposite-sign chirping of pump and Stokes pulses results in a lower two-photon intensity which is not sufficient for initiating AP.

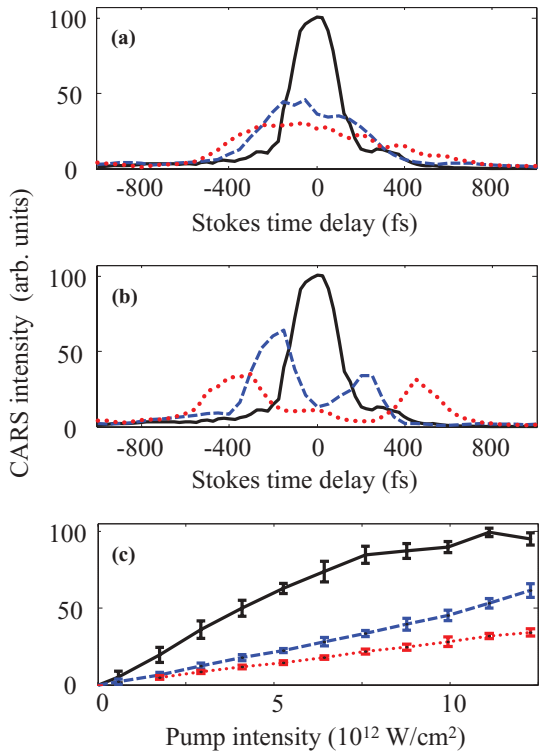

FIG. 14. (Color online) Near-resonance CARS. (a) CARS intensity as a function of pump-Stokes time delay for TL pulses (black solid line) and oppositely chirped pulses with $\alpha'_{S,p} = \pm 10\,000$ fs^2 (blue dashed line) and $\alpha'_{S,p} = \pm 25\,000$ fs^2 (red dotted line). (b) CARS intensity as a function of pump-Stokes time delay and (c) as a function of pump intensity with $I_S = 4 \times 10^{12}$ W/cm^2 for TL pulses (black solid line) and same-sign linearly chirped pulses with $\alpha'_{S,p} = -10\,000$ fs^2 (blue dashed line) and $\alpha'_{S,p} = -25\,000$ fs^2 (red dotted line).

In order to test the nonperturbative regime necessary for AP, we shift the central excitation wavelengths close to the electronic resonance [$\lambda_p = 645$ nm, $\lambda_S = 800$ nm, Fig. 3(c)]. This choice of wavelengths replicates that of Refs. [19,20]. In Fig. 14(a), the spectra of the excitation pulses are chirped linearly in opposite directions (RAP) with two different chirp amplitudes α'. CARS intensity is plotted as a function of the time delay between the pulses. We find no signatures of RAP (i.e., signal increase with frequency chirping at zero time delay) or STIRAP (i.e., signal increase with time delay at zero frequency chirp) and always record the strongest CARS signal with TL pump and Stokes pulses perfectly overlapping in time. From this observation, we conclude that no adiabatic evolution takes place.

In Figs. 14(b) and 14(c), we apply the successful same-sign frequency chirping, found in the off-resonance case, to the near-resonance interaction scheme. As discussed earlier, the two-photon spectrum becomes narrower and, depending on the exact pump-Stokes time delay, only one Raman transition is covered at a time [cf. Fig. 2(a)]. This is reflected by the peaks in the CARS intensity at certain time delays seen in Fig. 14(b). Figure 14(c) shows that for all beam intensities achievable in the experiment, the overall CARS intensity is lower than that for the unshaped pulses. Unlike the off-resonance case, pulse shaping does not improve the overall CARS efficiency. We attribute the difference to complicated dynamics due to one-photon coupling to the excited electronic state.

V. SUMMARY AND DISCUSSION

In this experimental and theoretical work, we investigated the utility of femtosecond pulse shaping to increase the efficiency of CARS in the strong-field excitation regime. We showed that when molecular eigenstates are significantly modified by the applied laser fields, the efficiency of exciting molecular vibration is no longer achieved with unshaped TL pulses. We analyzed two qualitatively different approaches to enhancing the magnitude of nonresonant vibrational excitation with shaped pulses.

In the first approach, pulse shaping was used to suppress strong-field effects, such as ac Stark shifts, while preserving the amplitude of the two-photon field at the frequency of Raman resonances. Numerically, we showed that linear frequency chirping of strong pump and Stokes pulses can provide several times better excitation efficiency than that achieved with TL pulses. The efficiency of Raman excitation with sinusoidal phase modulation showed an intermediate result. In the experiment, both techniques improved the strength of the observed CARS signal by 50% with respect to the TL case. Sinusoidal phase modulation resulted in a substantial signal gain while allowing us to excite a coherent vibrational wave packet, which may prove important in strong-field spectroscopic applications.

Multiple sets of pump and Stokes wavelengths were tested. Our main study was devoted to the far off-resonance case, where the dependence of vibrational excitation on the field parameters allows reasonably simple interpretation. In the near-resonance case, when either the ground or the target state were coupled to the excited electronic state, the population dynamics were erratic. In spite of the higher two-photon

Raman matrix elements, the excitation efficiency in all studied near-resonance cases was either negligibly higher or even substantially lower (depending on the choice of wavelengths) than in the far off-resonance case.

In the second approach, we put to test three AP scenarios which excel in a robust and efficient population transfer in simple two- or three-level atomic systems: RAP, STIRAP, and piecewise STIRAP [12,23,24]. All AP schemes studied in this work failed to establish an adiabatic evolution and did not improve the efficiency of Raman excitation. We associate this lack of success with two factors. Our numerical analysis showed that the complexity of the molecular spectrum prevents reaching the AP regime which is typically manifested by a high amount of population transferred to the target state or set of states. From the experimental point of view, AP requires shaping the excitation pulses in a way which reduces the two-photon spectral power density, making the available laser power insufficient for establishing an adiabatic evolution.

ACKNOWLEDGMENTS

The authors would like to thank Vladimir Malinovsky and Sergey Zhdanovich for valuable discussion. This work has been supported by DTRA Grant No. HDTRA1-09-1-0021.

[1] A. H. Zewail, *Femtochemistry* (World Scientific, Singapore, 1994).
[2] A. M. Weiner, Rev. Sci. Instrum. **71**, 1929 (2000).
[3] Y. Silberberg, Annu. Rev. Phys. Chem. **60**, 277 (2009).
[4] D. Meshulach and Y. Silberberg, Nature (London) **396**, 239 (1998).
[5] D. Meshulach and Y. Silberberg, Phys. Rev. A **60**, 1287 (1999).
[6] C. Trallero-Herrero, J. L. Cohen, and T. Weinacht, Phys. Rev. Lett. **96**, 063603 (2006).
[7] C. Trallero-Herrero and T. C. Weinacht, Phys. Rev. A **75**, 063401 (2007).
[8] M. Krug, T. Bayer, M. Wollenhaupt, C. Sarpe-Tudoran, T. Baumert, S. S. Ivanov, and N. V. Vitanov, New J. Phys. **11**, 105051 (2009).
[9] S. O. Konorov, J. W. Hepburn, and V. Milner, Phys. Rev. A **83**, 033417 (2011).
[10] R. S. Judson and H. Rabitz, Phys. Rev. Lett. **68**, 1500 (1992).
[11] M. O. Scully, G. W. Kattawar, R. P. Lucht, T. Opatrn, H. Pilloff, A. Rebane, A. V. Sokolov, and M. S. Zubairy, Proc. Natl. Acad. Sci. USA **99**, 10994 (2002).
[12] N. V. Vitanov, T. Halfmann, B. W. Shore, and K. Bergmann, Annu. Rev. Phys. Chem. **52**, 763 (2001).
[13] U. Gaubatz, P. Rudecki, S. Schiemann, and K. Bergmann, J. Chem. Phys. **92**, 5363 (1990).
[14] B. Broers, H. B. van Linden van den Heuvell, and L. D. Noordam, Phys. Rev. Lett. **69**, 2062 (1992).
[15] J. S. Melinger, S. R. Gandhi, A. Hariharan, D. Goswami, and W. S. Warren, J. Chem. Phys. **101**, 6439 (1994).
[16] V. A. Sautenkov, C. Y. Ye, Y. V. Rostovtsev, G. R. Welch, and M. O. Scully, Phys. Rev. A **70**, 033406 (2004).
[17] S. Zhdanovich, E. A. Shapiro, M. Shapiro, J. W. Hepburn, and V. Milner, Phys. Rev. Lett. **100**, 103004 (2008).
[18] T. Bayer, M. Wollenhaupt, and T. Baumert, J. Phys. B **41**, 074007 (2008).
[19] S. Gräfe, D. A. Akimov, B. Böhm, A. M. Zheltikov, M. O. Scully, W. Kiefer, V. Engel, and T. Siebert, J. Raman Spectrosc. **38**, 998 (2007).
[20] S. Gräfe, W. Kiefer, and V. Engel, J. Chem. Phys. **127**, 134306 (2007).
[21] J. Oreg, F. T. Hioe, and J. H. Eberly, Phys. Rev. A **29**, 690 (1984).
[22] V. S. Malinovsky and J. L. Krause, Eur. Phys. J. D **14**, 147 (2001).
[23] E. A. Shapiro, V. Milner, C. Menzel-Jones, and M. Shapiro, Phys. Rev. Lett. **99**, 033002 (2007).
[24] E. A. Shapiro, A. Peer, J. Ye, and M. Shapiro, Phys. Rev. Lett. **101**, 023601 (2008).
[25] S. Zhdanovich, E. A. Shapiro, J. W. Hepburn, M. Shapiro, and V. Milner, Phys. Rev. A **80**, 063405 (2009).
[26] T. Hellerer, A. M. K. Enejder, and A. Zumbusch, App. Phys. Lett. **85**, 25 (2004).
[27] A. M. Weiner, D. E. Leaird, G. P. Wiederrecht, and K. A. Nelson, Science **247**, 1317 (1990).
[28] J. Hauer, T. Buckup, and M. Motzkus, J. Chem. Phys. **125**, 061101 (2006).
[29] J. Hauer, H. Skenderovic, K.-L. Kompa, and M. Motzkus, Chem. Phys. Lett. **421**, 523 (2006).
[30] M. Wollenhaupt, A. Präkelt, C. Sarpe-Tudoran, D. Liese, T. Bayer, and T. Baumert, Phys. Rev. A **73**, 063409 (2006).
[31] J. Voll and R. d. Vivie-Riedle, New J. Phys. **11**, 105036 (2009).
[32] J. Konradi, A. K. Singh, A. V. Scaria, and A. Materny, J. Raman Spectrosc. **37**, 697 (2006).
[33] S. O. Konorov, X. G. Xu, J. W. Hepburn, and V. Milner, J. Chem. Phys. **130**, 234505 (2009).
[34] A. Abragam, *Principles of Nuclear Magnetism* (Oxford University Press, Oxford, 1961).
[35] K. P. Huber and G. Herzberg, *NIST Chemistry WebBook, NIST Standard Reference Database*, Vol. 69 of Constants of Diatomic Molecules (National Institute of Standards and Technology, Gaithersburg, MD, 2012).
[36] R. N. Zare, J. Chem. Phys. **40**, 1934 (1964).
[37] Raman line width for a train of pump-Stokes pulse pairs depends on the relation between $\tilde{\omega}_{p,S}$ in Eq. (2) and the central pump and Stokes frequencies $\omega_{0(p,S)}$. In the calculation shown in Fig. 4, the central Stokes wavelength is scanned while $\tilde{\omega}_S$ is fixed. In this scenario, the Raman line width at small intensities is as wide as that for a TL pulse.
[38] C. L. Yaws, *Handbook of Vapor Pressure*, 1st ed., Vol. 4 of Inorganic Compounds and Elements (Gulf Professional, Waltham, MA, 1995),
[39] D. Oron, N. Dudovich, and Y. Silberberg, Phys. Rev. Lett. **90**, 213902 (2003).
[40] A. C. Han and M. Shapiro, Phys. Rev. Lett. **108**, 183002 (2012).